Influence of plasma conditions on the defect formation mechanism in amorphous hydrogenated silicon

P. Kounavis,[a] D. Mataras, N. Spiliopoulos, E. Mytilineou,[a] and D. Rapakoulias
Department of Chemical Engineering, University of Patras, P. O. Box 1407, 26500 Patras, Greece

(Received 10 August 1993; accepted for publication 23 October 1993)

The variation of *a*-Si:H film quality, deposited by a rf glow discharge of pure silane, is examined as a function of the interelectrode distance for two different pressures. Constant photocurrent and modulated photocurrent methods are used to estimate the magnitude and the shape of the defect states in the valence band and the conduction band, respectively. An effort is made to correlate the film quality parameters and the defect formation with the plasma macroscopic and microscopic parameters. The results suggest that, at low interelectrode distances, high sticking coefficient radicals modify the film growth and the defect formation mechanisms, leading to the deterioration of the film quality. The conclusions drawn are compared with the predictions of recent theoretical models concerning the defect formation in *a*-Si:H.

I. INTRODUCTION

The influence of plasma conditions on the quality of the deposited *a*-Si:H film, and their importance on defect formation, is not directly evident. The exact mechanism through which plasma microscopic quantities (radicals, ions, photons, and electrons) interact with the film growth, still remains a subject of discussion. This is due to the limited amount of experimental data that correlate directly externally controllable, or *in situ* measured microscopic, plasma parameters to the electronic and structural properties of the film.

One often forgotten, but still very important, parameter is the discharge geometry, in terms of interelectrode distance, and powered-to-grounded surface area ratio. The influence of this parameter is not simple to evaluate, since the electric discharge symmetry also depends very strongly on the pressure and the power density. On the other hand, power density is, in general, calculated arbitrary, because most of the power fed by the generator is consumed in the matching network and in various in-line stray capacitances, which differ from system to system. Therefore only general trends can be obtained by the variation of this parameter. Which sometimes are only valid for the specific deposition system. It results that the only parameters that are accurately controlled today are pressure and flow rate. However, in order to overcome the problem of light induced degradation of the *a*-Si:H films one also has to search for deposition conditions that are outside the valley of the well known "best film quality" deposition conditions (low power, low pressure, sufficiently high temperature, low deposition rate). For this purpose one needs to have more accurate information about the influence of the basic discharge parameters to the plasma microscopic characteristics, and subsequently their correlation to the film quality.

Concerning the variation of interelectrode distance (D), which is the main subject addressed by this work, very little has been done during the past years. There are a few reports on the effect of D on the deposition rate and some properties of the films, in constant power density conditions,[1,2] while more recent works have addressed the same problem for the case of Germane.[3,4]

From the existing literature data one cannot have a clear opinion about the possible correlation of this parameter with the film quality. Therefore it is worth examining if the change in the film properties is due to the plasma parameters or to the speed of film growth and the after-growth processes. Recent theoretical models support the idea that a glass-like thermal equilibrium of the defect density occurs after the deposition.[5,6] The equilibrium state is established at a temperature below 300 °C, where the localized states in the energy gap are defined. Other models are considering some connection between plasma conditions and the electronic quality of the film. Thus, Winer[7] has formulated a model of the surface reactions, in which the critical parameter for optimal growth is the equilibrium between deposition rate and hydrogen diffusion. Alternatively, Street[8] has suggested that the hydrogen chemical potentials in the film and in the plasma will tend to equalize, and therefore optimal growth will occur if the hydrogen mobility is high enough to allow hydrogen equilibration in the growth zone. In these theories the substrate temperature (T_s) and the rf power are the most important deposition parameters for an optimum film growth. Thus, it is suggested that films with optimum quality should be deposited at a low deposition rate (< 1 Å/s).

In this work *a*-Si:H films were deposited at a substrate temperature and rf power within this optimum range. By varying the interelectrode distance and the pressure changes to the defect density and to the electronic properties of films are measured. The present results are correlated with the spatial distribution of active radicals in the reactor, which has been previously measured by this group.[9,10] The DOS distribution is calculated from CPM absorption spectra that measures optical transitions from occupied defect states at the valence band (VB) to the conduction band (CB) edge.[11] The energetic distribution of the localized states at the CB side is estimated from MPC measurements.[12]

[a]Department of Physics.

 0021-8979/94/75(3)/1599/8/$6.00

II. EXPERIMENT

All the *a*-Si:H films were deposited by 13.56 MHz glow discharge of pure silane at a substrate temperature of 250 °C. The 16 cm wide stainless steel chamber is equipped with two round 10 cm in diameter electrodes.[10] The rf electrode is fixed, while the grounded one is mounted on a linear motion vacuum feedthrough that permits continuous adjustment of the interelectrode distance. Furthermore, it incorporates a heating resistance and a *J*-type thermocouple, inserted through a cylindrical orifice (parallel to the electrode surface at a distance of 1 mm from it), which provides feedback to a PID temperature control loop (Eurotherm 093). The interelectrode distance (D) was varied between 20 and 35 mm. The rf power measured by a low-power SWR bridge, just after the matching network, was around 9 W. Since most of the power is believed to be consumed by the matching network and in-line stray capacitances, this measurement cannot be accurate and does not reflect the power dissipated in the discharge. Therefore, for reference, the value of the rf voltage was kept constant ($V_{pp}=-87$ V), while the value of the dc floating potential (V_{dc}) of the rf electrode was continuously measured.

The flow rate (18 sccm), and the pressure (50 or 100 mTorr), were independently adjusted by mass-flow controllers and downstream pressure control via a throttling valve. The deposition rate (R) was between 0.2 and 1.1 Å/s, depending on the interelectrode distance and pressure,[13] while all the films had a thickness of 0.9 μm. A base vacuum of 7×10^{-7} mbar was obtained before each deposition. The oxygen content of the films was measured by WDS (Wavelength Dispersion Spectroscopy). The level of oxygen contamination in the films was found to be in the range 0.6 to 0.9 at. % (~0.2 at. % surface oxygen included.)

The influence of preparation conditions to the film quality was studied by measuring the optoelectronic properties of the "as grown" samples. The effect of annealing was studied by heating the samples at 190 °C for 2 h in vacuum, followed by a very slow cooldown to the room temperature.

The output from a monochromator, equipped with a halogen lamp, was used as light source for the CPM measurements. The relative values of the absorption coefficient $a(E)$, obtained from CPM, were fitted on an absolute scale to the absorption measured from the optical transmission spectra.

The defect DOS above the Fermi level was measured by MPC. For this purpose a uniformly absorbed low intensity light (10^9–10^{11} photons cm^{-2} s^{-1}) of a LED, emitting at 660 nm, was used. The light intensity was sinusoidally modulated in the range of 5 Hz to 40 kHz. The amplitude [$i_{ph}(\omega)$] and the phase shift [$\Phi(\omega)$], between the resulting modulated photocurrent and the incident light beam waveforms, were measured by using a lock-in amplifier.[12]

III. RESULTS

A. Evaluation of the DOS

It is assumed that the most significant contribution to the CPM absorption spectra comes from the electron transitions to the conduction band. The defect DOS has been calculated from CPM absorption spectra according to the method of Jensen.[14] Additionally, the DOS was estimated by simulating the defect absorption spectra $a_d(E)$ using a hypothetical defect distribution. In this direction, the defect absorption spectrum is assumed to originate from a defect distribution that can be analyzed in two distinct Gaussian distributions:[15]

$$\alpha_d(E)=C\int N_c(E)\cdot N_d(E)\cdot f(E)dE, \tag{1}$$

where $N_c(E)$ is the DOS distribution above E_c, which is assumed to vary as the square root of energy (E), $f(E)$ is the Boltzmann distribution function, and N_d is the total defect density, taken as the sum of the two Gaussian distributions:

$$N_d(E)=D_1\exp-\frac{(E_c-E-E_1)^2}{2W_1^2}+D_2\exp-\frac{(E_c-E-E_2)^2}{2W_2^2}, \tag{2}$$

where D_1 and D_2 are the relative heights, E_1 and E_2 are the energies of the corresponding peak positions of the two distributions, and W_1 and W_2 are the half-width at half maxima (HWHM) of the peaks, respectively.

An estimation of the attempt-to-escape frequency (v_0) was made by measuring the variation of the phase shift with temperature and light intensity.[16] In all cases v_0 had a value between 5×10^{12} and 10^{13} s^{-1}. For simplicity, the value of 10^{13} s^{-1} was used for the determination of the energy scale for all the samples according to the following equation:

$$E_d(\omega)=kT\ln(v_0/\omega). \tag{3}$$

The defect DOS from room temperature MPC measurements was calculated according to the analysis of Bruggemann *et al.*:[17]

$$N_d=\frac{2}{\pi}\cdot\mathscr{E}\cdot A\cdot G_{ac}\cdot e\frac{\mu}{v\sigma}\cdot\frac{\sin\Phi}{i_{ph}(\omega)}, \tag{4}$$

where N_d is the defect density, $\mathscr{E}$ is the electric field, G_{ac} is the modulated electron generation rate, A is the conduction cross-sectional area of the sample, μ and v are the mobility and thermal velocity of carriers, and σ is the capture cross section of the traps. The scale factor $\mu/v\sigma$ for the determination of the absolute value of the DOS for the MPC method can be obtained by estimating the values of the free-carrier mobility and the capture cross section of the traps.[18] These parameters may be influenced by the variation of the preparation conditions, or even change from deposition to deposition, for the same preparation conditions. Therefore, the sensitivity of the phase-shift spectrum to the bias-light level was used to determine the above

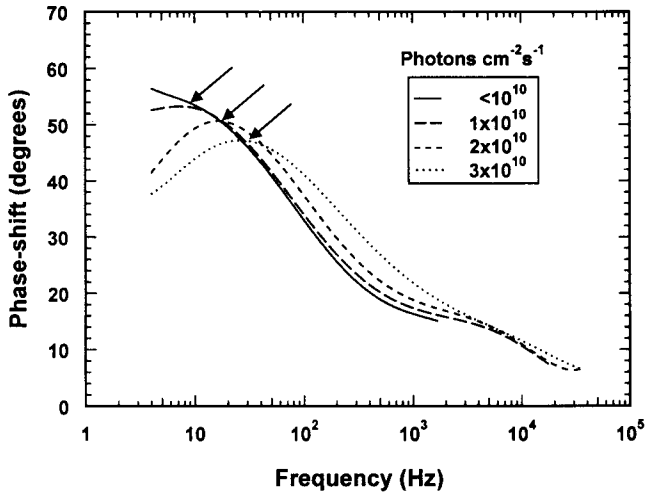

FIG. 1. Typical phase-shift spectra of a-Si:H at various light intensities.

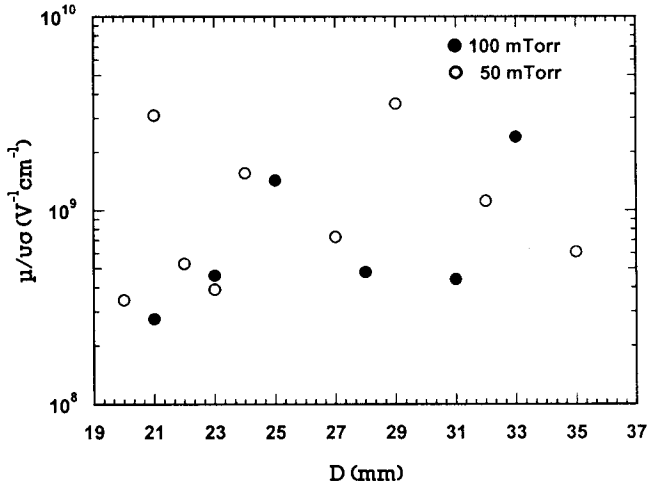

FIG. 2. The ratio $\mu/\upsilon\sigma$ as calculated from MPC, for films deposited at various D.

parameters. More specifically, the phase-shift spectrum was found to be sensitive to the bias-light intensity, as is illustrated in Fig. 1, which presents the phase shift as a function of frequency at different bias-light levels. One can observe that the phase-shift spectrum is almost independent of light intensity at small bias ($\leqslant 10^{10}$ photons cm^{-2} s^{-1}). In this case, thermal emission from traps dominates over recombination.[19] As the light bias is increased, the phase shift at low frequencies decreases, while at higher frequencies increases. A high bias-light increases the recombination rate, which in this case dominates over thermal emission from the deeper traps. At high bias-light levels ($>10^{10}$), the value of the angular frequency (ω_d) at which the phase shift presents a maximum ($10<\omega_d<100$ Hz, marked by arrows in Fig. 1), increases with the intensity of the bias light. The thermal emission rate at the specific ω_d frequency, for each bias-light level, is assumed to be equal to the capture rate, as can be expressed by the following equation:[18]

$$n \cdot \upsilon \cdot \sigma = \omega_d, \tag{5}$$

where n is the concentration of the free carriers produced by the bias light. By substitution of the known dc photoconductivity relation $\sigma_{\rm ph}=ne\mu$, the above equation can be written as

$$\kappa = \frac{\mu}{\upsilon\sigma} = \frac{\sigma_{\rm ph}}{e\omega_d}. \tag{6}$$

Therefore $\kappa=\mu/\upsilon\sigma$ can be calculated as the ratio of dc photoconductivity to the corresponding ω_d. The calculated values of the above ratio for different interelectrode distances and pressures are presented in Fig. 2. The estimated values of κ were found to be of the order of 10^9 V^{-1} s^{-1}, which is consistent with the values of $\mu=10$ cm^2 V^{-1} s^{-1}, $\upsilon=10^7$ cm s^{-1}, and $\sigma=10^{-15}$ cm^2 that are expected for a-Si:H.[20] The values of the above ratio were found to vary from preparation to preparation within a factor of ~ 5.

If a constant κ ratio is used, MPC can give up to one order of magnitude higher DOS, particularly in the most defective samples.[21] On the contrary, if the estimated values of κ are considered, both CPM and MPC methods give comparable DOS values for all the samples.

B. Influence of interelectrode distance (D)

Figure 3 presents the energy distribution of the deep defect DOS of a-Si:H films deposited at 100 mTorr and at interelectrode distances of 21, 25, 28, and 33 mm. The defect density of the VB was calculated from the CPM measurements, while that of the CB from the MPC measurements, using the κ value calculated for each sample. It is observed that DOS is increased at lower D for both bands. The same general effect can be observed for films deposited at 50 mTorr and interelectrode distances of 21, 23, 29, 32, and 35 mm (Fig. 4). The CPM spectra, as well as the corresponding DOS (Figs. 3 and 4), show evidence of two distinguished defect distributions located approximately at 0.9 and 1.2 eV from E_c. Using the method of

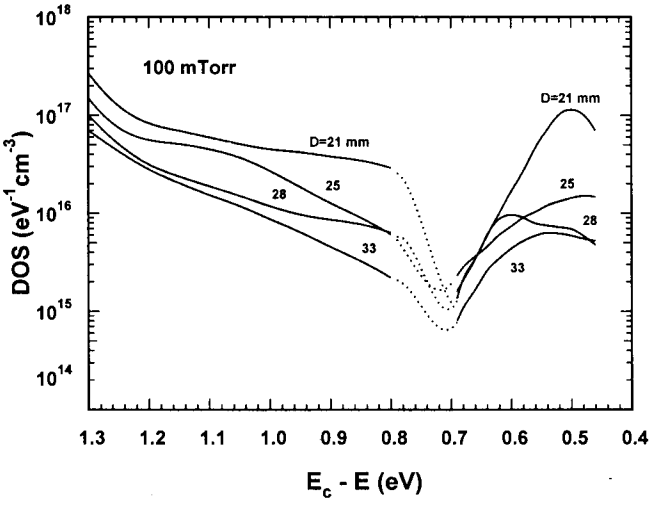

FIG. 3. DOS distribution within the energy gap of films deposited at various D and 100 mTorr of pure silane from CPM and MPC. (Dotted lines are drawn as a visual aid.)

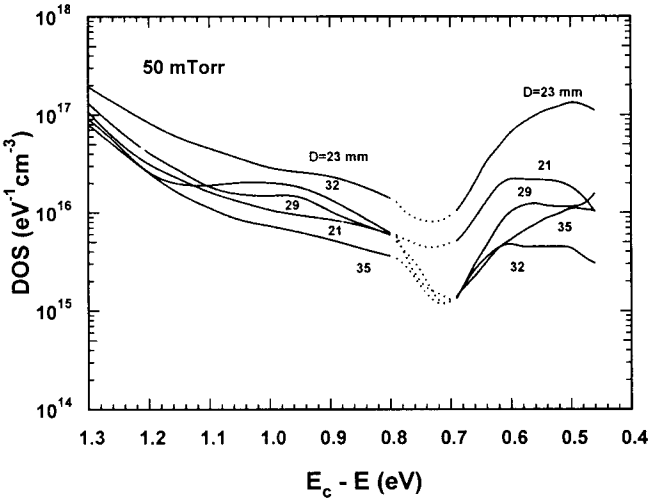

FIG. 4. DOS distribution within the energy gap of films deposited at various D and 50 mTorr from CPM and MPC. (Dotted lines are drawn as a visual aid.)

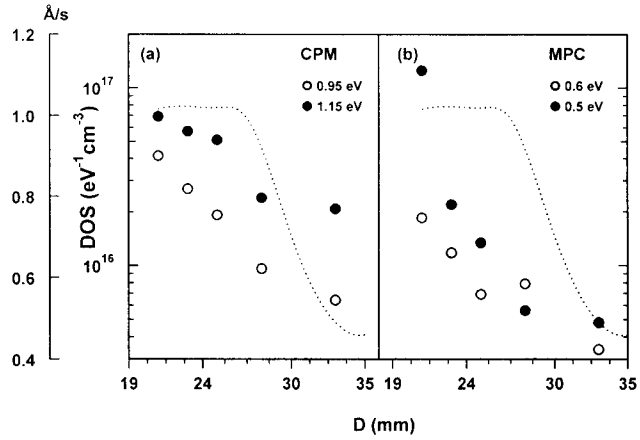

FIG. 5. DOS at 1.15 and 0.95 eV from (a) CPM and at 0.6 and 0.5 eV below E_c from (b) MPC, for films deposited at 100 mTorr. Dotted lines show the variation of the deposition rate with D.

Vanecek *et al.*,[11] and assuming two Gaussian defect distributions,[15] an excellent fit to the defect absorption is obtained. The calculated DOS according to this method is in very good agreement with that obtained according to the analysis of Jensen,[14] where no assumptions were made about the number or the shape of the defect distributions. The best fit to the defect absorption is obtained when the defect distribution peaks are located between 0.95–1 eV and 1.15–1.2 eV, depending on the preparation conditions, with HWHM values of 0.13 and 0.09 eV, respectively. Nevertheless, in some samples (D=32, 29 in Fig. 4 and D=27 mm not shown), there is only one intense peak at 1–0.95 eV which dominates over the whole energy distribution. In this case the defect absorption can be reproduced from a simulation using a single Gaussian distribution.

The defect states on the CB side also show evidence of two defect distributions at 0.5 and 0.6 eV from E_c, as indicated from MPC measurements. However, in Figs. 3 and 4 one can observe that for the samples with the highest defect density, the DOS from MPC is larger than that from CPM, while for the rest of the samples MPC gives equal or lower DOS. In this context one must also take into account that the CPM defect density calculations are sensitive to the relative positions of the Fermi level and the defect band, which are not known.[22] The discrepancy between the two methods would probably be reduced if one could take into account the respective capture coefficient, as was done for the MPC, and the distance of the Fermi level from the defect band.

The variation of the defect DOS at the VB, at 1.15 and 0.95 eV, and that of the CB (at 0.6 and 0.5 eV below E_c), are plotted in Figs. 5(a) and 5(b), respectively, as a function of the interelectrode distance for films deposited at 100 mTorr, shown together with the variation of the deposition rate. The total DOS distribution of both bands increases gradually as the interelectrode distance is reduced. Similarly, Figs. 6(a) and 6(b) show the variation of the DOS at the corresponding defect levels specified above, as a function of the interelectrode distance for samples prepared at 50 mTorr. In this case, the defect DOS of both bands shows a much stronger dependence on the interelectrode distance. In this series of samples, the ones deposited at a 22–23 mm interelectrode distance and 50 mTorr pressure show the highest defect DOS, while those prepared at $D \geqslant 29$ mm, independent of pressure, show the lowest DOS. The general trend of increase of the DOS with interelectrode distance, observed in these results for both 50 and 100 mTorr, has one systematic exception for $D < 22$ mm and 50 mTorr, which will be further discussed. One must note that annealing reduces the peak intensities at 0.6 and 0.95 eV by a factor of 2 while it does not significantly change the other two peaks. This behavior indicates the metastable character of these defects.

CPM spectra can give further information on the way the defect density of the films is influenced by the change of D, if one takes into consideration the above-bandgap absorption region. Thus, Fig. 7 shows the variation of $1/f, f$ being the photon flux necessary to maintain a constant

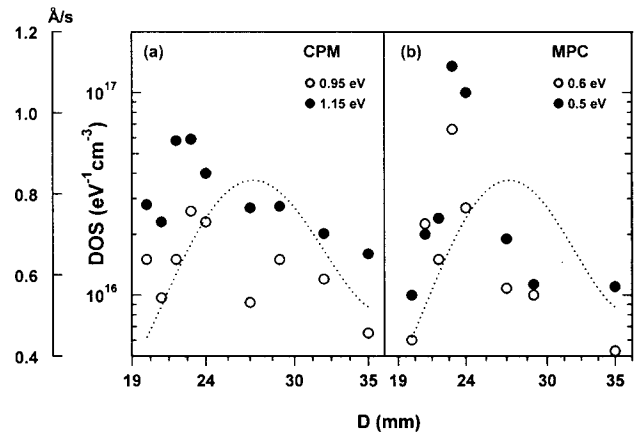

FIG. 6. DOS at 1.15 and 0.95 eV from (a) CPM and at 0.6 and 0.5 eV below E_c from (b) MPC, for films deposited at 50 mTorr. Dotted lines show the variation of the deposition rate with D.

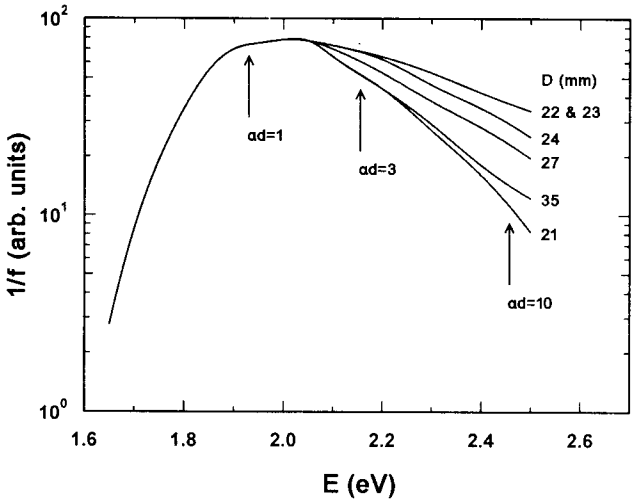

FIG. 7. CPM spectra for photon energies above the bandgap, for films deposited at various D and 50 mTorr.

photocurrent, as a function of the photon energy, for films deposited at various D and 50 mTorr. These curves can be considered as a depiction of the relative defect depth profile from the bulk to the surface of the film. The observed decrease of the $1/f$ is most probably due to the increase of the number of recombination centers at the corresponding absorption depth ($1/a$), when going from the bulk toward the surface of the film. The relative increase of the surface defect density is systematically steeper for samples grown at large D, while the opposite is true for samples grown at low D, again with the exception of samples deposited at $D<22$ mm. The same effects can be observed for films grown at 100 mTorr. One must note that annealing tends to normalize the $1/f$ curve toward the value corresponding to $ad=1$, and is more effective on the samples with the steeper bulk-to-surface defect increase.

For reference reasons, in Fig. 8 is presented the value of V_{dc} as a function of the interelectrode distance for 50

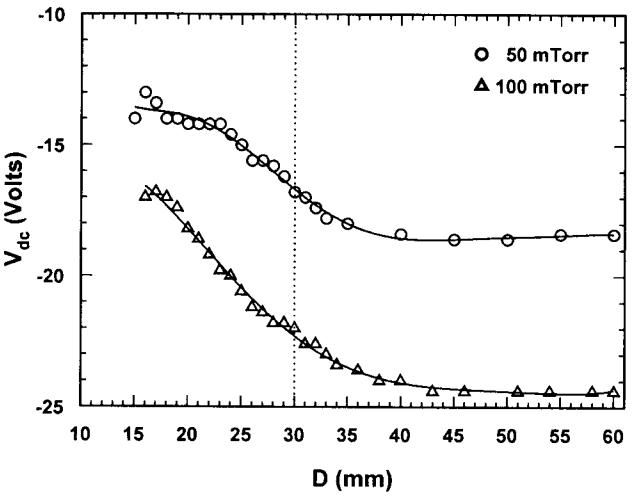

FIG. 8. Self-bias dc potential of the rf electrode V_{dc} as a function of D for 50 and 100 mTorr. The dotted line indicates the distance between the electrode edge and the chamber walls.

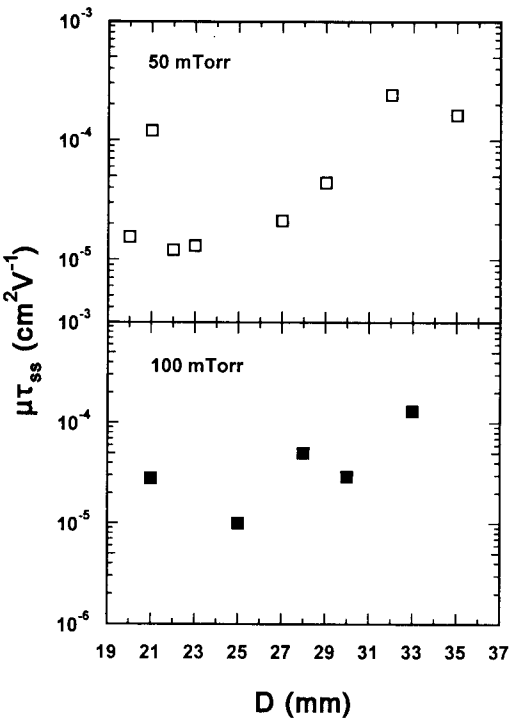

FIG. 9. The $\mu\tau_{ss}$ product calculated from steady-state photoconductivity ($\lambda=620$ nm) as a function of D.

and 100 mTorr. One can observe the increase of V_{dc} with increasing D and decreasing pressure. This increase is indicative of the decreasing electrical symmetry of the discharge (the powered to grounded area ratio), which generally decreases with pressure. Additionally, at D comparable to the distance between the electrodes and the grounded chamber walls, the discharge becomes even more asymmetric.

C. Variation of the transport properties with D

The room temperature photoconductivity, for all the samples, was between 10^{-7} and 10^{-5} Ω^{-1} cm^{-1}, while the dark conductivity varied between 10^{-11} and 10^{-10} Ω^{-1} cm^{-1}. The value of the optical gap was found to be always in the range of 1.7–1.75 eV, which is consistent with the almost constant value of the hydrogen content of about 7%–12% that was obtained from hydrogen evolution measurements.

Figure 9 display the $\mu\tau_{ss}$ product, calculated from the steady-state photoconductivity for a photons flux of 10^{14} photons cm^{-1} s^{-1} at 620 nm, as a function of D for films prepared at 50 and 100 mTorr. In both pressures a slight decrease of $\mu\tau_{ss}$ is observed with the decrease of D. More specifically, as can be seen from Figs. 5 and 6, the proposed reduction of the $\mu\tau_{ss}$ is consistent with the respective enhancement of the defect density. Consequently, the decrease of the $\mu\tau_{ss}$ product is most probably associated with the increase of the recombination of the free carriers at deep defect states, as the DOS increases at low D.

From the present results, describing the optoelectronic properties of the samples, one cannot have direct informa-

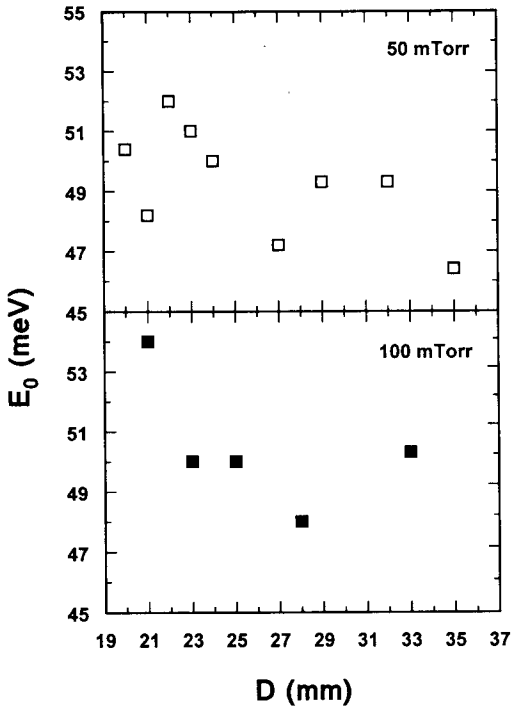

FIG. 10. The characteristic slope E_0 of the valence band obtained from the absorption edge measured by CPM.

tion about eventual modifications of the film microstructure with D. However, as results from Fig. 10, the characteristic slope of the valence band is rather insensitive to the variation of D; E_0, which gives a macroscopic measure of the disorder of the a-Si:H network, is about 50 meV independent of D.

IV. DISCUSSION

The results presented here show a direct relation between interelectrode distance D and the defect DOS and deposition rate. In general, this indicates that the specific plasma conditions play an important role in defect formation. The main observable effect is that the decrease of D increases the defect DOS, and this effect is more pronounced at lower pressures. However, at lower pressures the DOS presents a maximum for $D=23$ mm and then drops again. The explanation of the phenomena observed here is not straightforward due to the complexity of the influence of D to the plasma characteristics. The variation of D, while keeping a constant total power, modifies several microscopic plasma parameters, depending on the discharge symmetry.[10] The power density increases with D^{-1} thus increasing the mean electron density and electron temperature. This is mainly due to the fact that the contribution of the sheaths to the overall discharge volume increases, since the magnitude or the shape of the sheaths does not change with D. Therefore there is an enhanced contribution of sheath related fast electrons (either secondary or wave riding) that modify the shape of the electron energy distribution in space. This change favors higher energy electron–collision processes (ionization, excitation, high energy dissociation) against the low energy ones (lower energy dissociation, momentum transfer). Indeed, previous work of this group has indicated that there is a redistribution of the energy consumption between high energy processes and lower energy ones.[10] More specifically, simultaneous laser induced fluorescence (LIF) and optical emission spectroscopy (OES) measurements have shown that the overall intensity of both the ground-state SiH and the excited state SiH* radicals, as well as the SiH*/SiH ratio, increase at smaller D.

A direct consequence of the redistribution of energy consumption is the increase of the high sticking coefficient to the low sticking coefficient radicals flux ratio. Namely, the relative abundance of each radical and their role in the film growth process will be modified at high power densities.[23] If one takes into account the main dissipation reactions of SiH_2 and SiH_3,

$$(R_1)\ \ SiH_2+SiH_4\rightarrow Si_2H_6\ k_1=1\times10^{-11}\ \text{cm}^3/\text{s},^{24}$$

$$(R_2)\ \ SiH_3+SiH_3\rightarrow Si_2H_6\ k_2=1.5\times10^{-10}\ \text{cm}^3/\text{s};^{25}$$

it results that low power density will lead to higher SiH_3/SiH_2 flux ratio to the surface (radical–radical reactions are less important[23]), which additionally will increase at larger interelectrode distances because of the fast reaction rate of SiH_2 with silane (R_1).[26] The opposite is true at high power densities (low distances) when SiH_3–SiH_3 (R_2) reactions become important, while SiH_2 and the other "sticky" radicals have enhanced possibilities to reach the surface. Calculations of the total possibility of each radical to reach the anode surface have indicated that this effect is predominantly influencing the anodic deposition.[13] This is because the production of radicals is inhomogeneous in space, and at these conditions the location of the radicals generation profile in space does not depend on the location of the grounded electrode.

Therefore, high-sticking coefficient radicals (Si, SiH, SiH_2) at lower D have an enhanced probability to arrive at the growing film surface, and begin to have a significant participation to the film growth mechanism. This phenomenon is much more important at lower pressures, where the diffusion/reaction lifetime ratio of these radicals is higher. These low mobility radicals are incorporated in the film network at or very near the position where they are adsorbed. This situation alters the film growing mechanism, and, for high enough numbers of "sticky" radicals, may lead to structural irregularities that cannot be accommodated anymore by the normal film structure. For the case of the 50 mTorr curves (Fig. 6), an additional phenomenon is involved at very low distances. The presence of the maximum and the slight amelioration of the DOS for $D<23$ mm observed in these data can be due to the fact that at low distances and low pressures the electron density drops because of the enhanced depletion of electrons striking the electrode surfaces. It has been observed by LIF measurements that this influences only the ground state radicals generation rate.[10] Additionally, the same behavior has been observed for the influence of D to the deposition rate.[13] However, other changes in the plasma conditions,

such as the enhancement of silane depletion or ion bombardment, can also be the cause, at least partially, for this behavior.

Concerning the various defect formation models that have been proposed, the results presented here can be interpreted as follows. According to the weak bond–dangling bond conversion model, an enhancement of the defect density is expected when a number of weak bonds from the valence band tail exceeding an energy demarcation level (E_{db}) are converted spontaneously to dangling bonds.[27] As the characteristic slope of the valence band tail is almost constant in these samples, an increase of the defect DOS at low D can be explained by a shift of the E_{db} toward the VB. Thus, at higher D, in both pressures examined here, E_{db} is estimated[27] to be about 0.39–0.41 eV, while at low D it is about 0.34–0.36 eV from the VB. This can be explained by the hypothesis that the local microstructure of the films deposited at low D, favors the formation of a number of undercoordinated atoms instead of weak bonds.

The explanation given for the experimental results is in agreement with the model proposed by Hata *et al.*[28] As was explained earlier, the growing network cannot accommodate more than a certain number of "sticky" radicals producing surface irregularities, and this results in an excessive number of defects. Therefore the annealing energy barrier is large and cannot be met by the given temperature or ion bombardment conditions.[29,30] Thus, films grown in low D conditions do not present large differences between bulk and surface defects, as shown in Fig. 7, while at large D the bulk defect is reduced by annealing during the growth of the film.

On the contrary, although the samples presented here are grown under low deposition rate conditions (< 1 Å/s), which is believed to be sufficiently low in order to allow the accommodation of defects, according to the model of Winner,[7] there is an evident relation between the plasma conditions and the defect density. Moreover, the deposition rate varies with D with a different trend than the DOS (Figs. 5 and 6).

V. CONCLUSION

An effort was made to link some macroscopic plasma characteristics to the *a*-Si:H film electronic properties. It was found that the electronic properties and the DOS characteristics, i.e., the magnitude and the shape of the various defect bands within the energy gap, are strongly influenced by the interelectrode distance, D. More specifically, when D decreases the defect density increases, while the deposition rate is changing in a different way, suggesting that the film growth rate and the defect formation mechanism are influenced by the plasma conditions. These observations are correlated with the previous work of this group regarding the influence of discharge geometry to the radical generation mechanism. It is suggested that at low D high sticking coefficient radicals, which are expected to have a larger contribution to the film growth under these conditions, produce surface irregularities, thus altering the film microstructure. The situation can be improved by the increase of ion bombardment that increases the radical surface mobility. Thus, in both ways, plasma conditions have significant influence on critical parameters that define the defect density characteristics and thus the film properties. The results presented here do not show any systematic correlation to the deposition rate, which, in any case, is lower than 1 Å/s. Thus, the change of the film electronic properties cannot be explained by a hydrogen diffusion bottleneck. To the contrary, the suggested modification of the microstructure results in an annealing barrier that cannot be met by the specific energetic conditions during the growth.

ACKNOWLEDGMENTS

The authors wish to thank W. Beyer for the hydrogen effusion measurements, and W. Fuhs and P. Roca i Cabarrocas for the helpful discussions. This work was financially supported by the JOULE I and II programs of the EEC DG XII.

[1] R. C. Ross and J. Jaklik Jr., J. Appl. Phys. **55**, 3785 (1984).
[2] S. I. Ishihara, M. Kitagawa, T. Hirao, K. Wasa, T. Arita, and K. Mori, J. Appl. Phys. **62**, 485 (1987).
[3] F. H. Karg, H. Bohm, and K. Pierz, J. Non.-Cryst. Solids **114**, 477 (1989); F. H. Karg, B. Hirschauer, W. Kasper, and K. Pierz, Sol. Energy Mater. **22**, 169 (1991).
[4] P. Wickboldt, S. J. Jones, F. C. Marques, D. Pang, W. A. Turner, A. E. Wetsel, W. Paul, and J. H. Chen, Philos. Mag. B **64**, 655 (1991).
[5] R. A. Street and K. Winner, Phys. Rev. B **40**, 6236 (1989).
[6] K. Pierz, W. Fuhs, and H. Mell, Philos. Mag. B **63**, 123 (1991).
[7] K. Winner, Phys. Rev. B **41**, 12 150 (1990).
[8] R. A. Street, Phys. Rev. B **43**, 2454 (1991).
[9] D. Mataras, S. Cavadias, and D. Rapakoulias, J. Appl. Phys. **66**, 119 (1989).
[10] D. Mataras, S. Cavadias, and D. Rapakoulias, J. Vac. Sci. Technol. A **11**, 664 (1993).
[11] M. Vanecek, J. Kocka, J. Stuchlik, Z. Kozisek, O. Stika, and A. Triska, Sol. Energy Mater. **8**, 411 (1983).
[12] P. Kounavis and E. Mytilineou, J. Non-Cryst. Solids **137&138**, 955 (1991).
[13] D. Mataras, D. Rapakoulias, P. Kounavis, and E. Mytilineou, in *Proceedings of the 10th European Photovoltaic Solar Energy Conference*, Lisbon, 1991, edited by A. Luque, G. Sala, W. Palz, G. Dos Santos, and P. Helm (Kluwer, Dordrecht, 1991), p. 165.
[14] P. Jensen, Solid State Commun. **76**, 1301 (1990).
[15] I. Sakata, M. Yamanaka, S. Numase, and Y. Hayashi, J. Appl. Phys. **71**, 4344 (1992).
[16] C. Main, D. P. Webb, R. Bruggemann, and S. Reynolds, J. Non-Cryst. Solids **137&138**, 951 (1991).
[17] R. Bruggemann, C. Main, J. Berkin, and S. Reynolds, Philos. Mag. B **62**, 29 (1990).
[18] P. Kounavis and E. Mytilineou, J. Non-Cryst. Solids (to be published).
[19] J. P. Kleider, C. Longeaud, and O. Glodt, Phys. Rev. B **45**, 11 672 (1992).
[20] R. A. Street, Appl. Phys. Lett. **41**, 1060 (1982).
[21] P. Kounavis, N. Spiliopoulos, D. Mataras, E. Mytilineou, and D. Rapakoulias, in *Proceedings of the 11th European Photovoltaic Solar Energy Conference* Montreux 1992, edited by L. Guimaraes, W. Palz, C. De Reyff, H. Kiess, and P. Helm (Harwood, London, 1992), p. 726.
[22] R. H. Bube, L. E. Benatar, M. N. Grimbergen, and D. Redfield, J. Appl. Phys. **72**, 5766 (1992).
[23] M. J. Kushner, J. Appl. Phys. **62**, 2803 (1987).
[24] A. Gallagher, J. Appl. Phys. **63**, 2406 (1988).
[25] N. Itabashi, K. Kato, N. Nishiwaki, T. Goto, C. Yamada, and E. Hirota, Jpn. J. Appl. Phys. **27**, L1565 (1988); N. Itabashi, K. Kato, N. Nishiwaki, T. Goto, C. Yamada, and E. Hirota, *ibid.* **28**, L325 (1989).
[26] M. J. Kushner, J. Appl. Phys. **63**, 2532 (1988).

[27] M. Stutzmann, Philos. Mag. B 60, 531 (1989).
[28] N. Hata, S. Wagner, P. Roca i Cabarrocas, and M. Favre, Appl. Phys. Lett. 56, 2448 (1990); N. Hata and S. Wagner, J. Appl. Phys. 72, 2857 (1992).
[29] P. Roca i Cabarrocas, Y. Bouizem, and M. L. Theye, Philos. Mag. B 65, 1025 (1992).
[30] P. Roca i Cabarrocas, P. Morin, V. Chu, J. P. Conde, J. Z. Liu, H. R. Park, and S. Wagner, J. Appl. Phys. 69, 2942 (1991).